Restoring the pattern of perineuronal net sulphation corrects age-related memory loss

Sujeong Yang[1*], Sylvain Gigout[2§], Angelo Molinaro[3§], Yuko Naito-Matsui[4], Sam Hilton[1], Simona Foscarin[1], Bart Nieuwenhuis[1,5], Joost Verhaagen[5], Tommaso Pizzorusso[3,8], Lisa M. Saksida[6], Timothy M. Bussey[6], Hiroshi Kitagawa[4], Jessica C.F. Kwok[2,7*], James W. Fawcett[1,7*]

Affiliations:

[1] Dept. Clinical Neurosciences, John van Geest Centre for Brain Repair, University of Cambridge, Cambridge CB2 0PY, UK

[2]School of Biological Sciences, Faculty of Biological Sciences, University of Leeds, Leeds LS2 9JT, UK

[3]Institute of Neuroscience, CNR, Via Moruzzi 1, 56124 Pisa, Italy

[4]Department of Biochemistry, Kobe Pharmaceutical University, Kobe, Japan

[5]Laboratory for Regeneration of Sensorimotor Systems, Netherlands Institute for Neuroscience, Royal Netherlands Academy of Arts and Sciences (KNAW), 1105 BA Amsterdam, The Netherlands

[6] Molecular Medicine Research Group, Robarts Research Institute, Schulich School of Medicine & Dentistry, Western University, London, Ontario, Canada

[7] Centre for Reconstructive Neuroscience, Institute of Experimental Medicine, Prague 14220, Czech Republic

[8] Department NEUROFARBA, University of Florence, Florence Italy

*Correspondence to:

James Fawcett, John van Geest centre for Brain Repair, University of Cambridge, Cambridge CB2 0PY, UK. Email: jf108@cam.ac.uk, Tel: +441223331188, Fax +331223 331174

Jessica Kwok, School of Biomedical Sciences, Faculty of Biological Sciences, University of Leeds, LS2 9JT, UK. Email:j.kwok@leeds.ac.uk, Tel: +44113 3439802

Sujeong Yang, John van Geest centre for Brain Repair, University of Cambridge, Cambridge CB2 0PY, UK. Email:sjy25@cam.ac.uk, Tel:+441223336633

§ These authors contributed equally to the work

Acknowledgements: Funding for this study was a fellowship to SY from Alzheimer's Research UK (ARUK-RF2016A-1), ARUK Yorkshire Network and Medical Research Council CiC, , to JCFK and JWF from European Research Council, CZ.2.1.01/0.0/0.0/15_003/000419, Medical Research Council .

Short title: PNN sulphation corrects restores memory loss

One sentence summary: Sulphation changes in perineuronal nets lead to age-related memory loss; correction of sulphation restores memory.

Abstract

Memory loss is a usual consequence of ageing. In aged brains, perineuronal nets (PNNs), which limit neuroplasticity and are implicated in memory, become inhibitory due to decreased 6-sulphation of their glycan chains (C6S). Aged mice show progressive deficits in memory tasks, but removal of PNNs or digestion of their glycans rescued age-related memory loss. Reduction of permissive C6S by transgenic deletion of 6-sulfotransferase led to very early memory loss. However, restoring C6S levels in aged animals by AAV delivery or transgenic expression of 6-sulfotransferase restored memory. Low C6S levels caused loss of cortical long-term potentiation, which was restored by AAV-mediated 6-sulfotransferase delivery. The study shows that loss of

C6S in the aged brain leads to declining memory and cognition, which can be restored by C6S replacement.

Results and Discussion

Diminished ability to form and retrieve memories is a usual consequence of ageing and current treatments for memory restoration are inadequate. Various explanations for memory loss have been proposed, including synaptic loss, neuronal dysfunction, oxidative stress, loss of myelin and others (*1*). Here, we demonstrate a role for the CNS extracellular matrix (ECM) in age-related memory loss, and show that ECM manipulation can rescue memory. Previous work points to a key role for chondroitin sulphate proteoglycans (CSPGs) in memory. Memory acquisition is associated with formation of new inhibitory inputs to GABAergic parvalbumin$^+$ (PV$^+$) neurons (*2-4*). The somata and dendrites of most of these PV+ neurons are surrounded by perineuronal nets (PNNs), condensed extracellular matrix structures that surround synapses and are involved in the control of developmental and adult plasticity (*5-8*). Digestion of inhibitory CSPGs (the main effectors of PNNs) with chondroitinase ABC (ChABC), enables increased formation of inhibitory synapses on PV$^+$ neurons (*2, 9*), and enhances memory formation and duration in young animals, as does transgenic attenuation of PNNs (*10, 11*). Moreover in animals with defective memory due to pathology from mutant tau or amyloid-beta, CSPG digestion or antibody treatment to block inhibitory 4-sulphated CS-GAGs restores memory to normal levels (*12-14*). Together these previous results demonstrate a role for PNNs in memory, and show that PNN CS-GAGs are the key component (*15*). The binding properties and function of GAGs are

determined by their pattern of sulphation. This pattern changes with age; at birth PNN GAGs are 18% 6-sulphated (C6S), at the end of critical periods C6S declines to 4%, then in aged rats there is an almost complete loss of C6S (*16, 17*) leading to an increase in ratio of C4S/C6S. C6S is permissive to axon growth and plasticity (*18, 19*), so this developmental change results in PNN matrix becoming much more inhibitory in aged brains (*16*). Our hypothesis was that aged PNNs which have become more inhibitory due to loss of C6S, lead to memory loss associated with diminished inhibitory synapse formation onto PV^+ interneurons.

We first established that aged 20 month-old (20M) mice have a progressive memory and cognitive deficit compared to young 6 month-old mice (6M) using three tests. Spontaneous object recognition (SOR) (which depends on the perirhinal cortex (PRh), allowing focal application of treatments), spontaneous alternation (SA) (which tests hippocampal-dependent spatial memory), and marble burying (MB) (a test of species-typical behaviour, related to hippocampal function). In aged 20M animals, C57/Bl6 mice showed loss of SOR memory (6 hr recall, Fig 1A), and declines in SA (Fig. S3E) and in MB (Fig S1C). Baseline object exploration in the tasks remained normal (Fig.S1A) indicating cognitive decline rather than a gross motor or attention deficit. To investigate a link between CSPGs and SOR memory loss in the aged brain, we digested CS-GAGs by injecting ChABC into the PRh in 20M animals. This restored SOR memory, but memory declined again as the digested CSPGs were renewed and was defective again by 6 weeks after treatment (Fig. 1B, timeline Fig S1D). SA and MB (which do not specifically depend on PRh) were not affected by this focal treatment. The increased inhibitory inputs to PV^+ interneurons during memory acquisition have been shown to lead to a decrease in PV and GAD67 levels indicating decreased GABA production in young animals (*2*). ChABC-mediated PNN digestion similarly increases inhibitory inputs and decreases PV expression (*2,*

20). At 20M we saw an increase in the proportion of PV cells that express high PV in the aged cortex compared to 6M (Fig. 1C). ChABC treatment at both ages increased low-expressing and decreased high expressing neurons (Fig 1D). The overall number of PV^+ neurons and PNNs in PRh was unchanged by ageing (Fig S1B).

ChABC treatment implicates CS-GAGs on CSPGs, but only ~2% of CSPGs are in PNNs (*21*). To link memory loss to PNNs, we measured memory loss in animals with attenuated PNNs due to deletion of the PNN-associated *hapln1* link protein. In non-aged *hapln1* knockouts, memory is prolonged and various forms of plasticity are enhanced (*17*). We tested SOR in these knockout animals at time points up to 20M. Even at 20M, these animals showed no loss of SOR memory, with memory extended to 48hr (Fig 1E). Together, these results suggest that the CS-GAGs of CSPGs in PNNs are involved in the loss of SOR memory in aged mice.

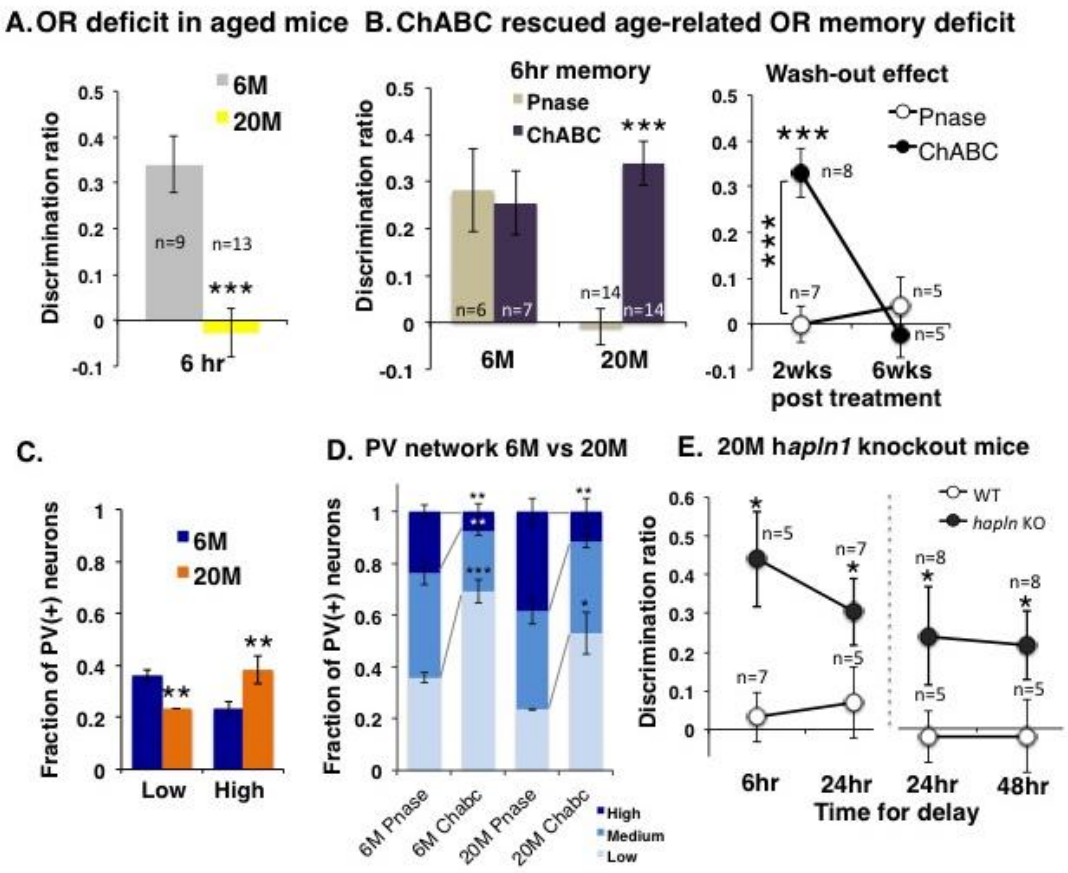

Fig.1 Involvement of CSPGs and PNNs in aged memory

(A) OR memory deficit in aged mice. Unpaired two-tailed t-test, ***p=0.0002 (B) ChABC injection rescued age-related OR memory deficit. 6hr memory, unpaired two-tailed t-test, *** p=0.0001. Wash-out of ChABC treatment effect of 6 hr memory in 20M mice. 2-Way ANOVA interaction treatment x time, ***p<0.001. Main effect of Time: ** p<0.01. Treatment: ** p<0.01. Bonferroni posthoc test, ChABC 2wks vs 6wks, ***p<0.001. 2wks Pnase vs ChABC, ***p=0.0002. (C) 6M vs 20M Low PV: **p=0.0012, High PV **p=0.0061, n=6/group, Data present as mean ± SEM. (D) PV network modification after ChABC treatment in 6M vs 20M old mice 6M Pnase vs ChABC n=6/group, Low: ***p<0.0001 Medium: **p=0.0027 High: **p=0.0028, 20M Pnase vs ChABC n=4/group, Low: *p=0.019 High: **p=0.0099 (E) NOR memory in aged *hapln1* KO mice. Unpaired two-tailed t-test. 6hr delay: *p=0.0094. 24hr delay: *p=0.032, *=p=0.0226. 48hr delay: *p=0.0145 48hr delay: *p=0.0295.

Our hypothesis was that the loss of C6S in the CS-GAGs of aged PNNs makes them increasingly inhibitory to axon growth and plasticity, leading to defective memory in the aged brain. As in a

previous study in rats (*16*), we found that in aged 20M mice C6S levels become low, the ratio of C4S to C6S increased by 56% in PNN extracts. If C6S is a causal factor in age-related memory loss, a decrease in C6S at any age might be expected to lead to memory loss, while restoring C6S levels should restore memory. To test whether premature C6S loss affects memory, SOR, SA and MB were tested in C6 sulfotransferase-1 (*chst3*) knockout animals in which C6S is greatly diminished (*22*). At 8 weeks of age (8W) SOR memory formation and retention were normal, but by 11W there was a clear deficit and by 13W there was no measurable memory retention at 3hrs (Fig. 2A). These animals also showed defective spatial memory as measured by SA by 4 months of age (Fig. 2B, fig. S2B), and defective marble burying (Fig.2C). The number of PNNs was normal in these mice (Fig.S2C).

To test whether restoration of C6S could recover memory in *chst3* knockout mice, an AAV1 vector expressing mouse *chst3* under a PGK promoter was injected into the PRh at 4 months of age. Injected brains were stained with the anti-C6S antibody CS56, demonstrating an increased C6S level in the injected region associated with PNNs and other structures (Fig. S3D). SOR memory was restored in AAV-*chst3*- injected animals (Fig.2D).

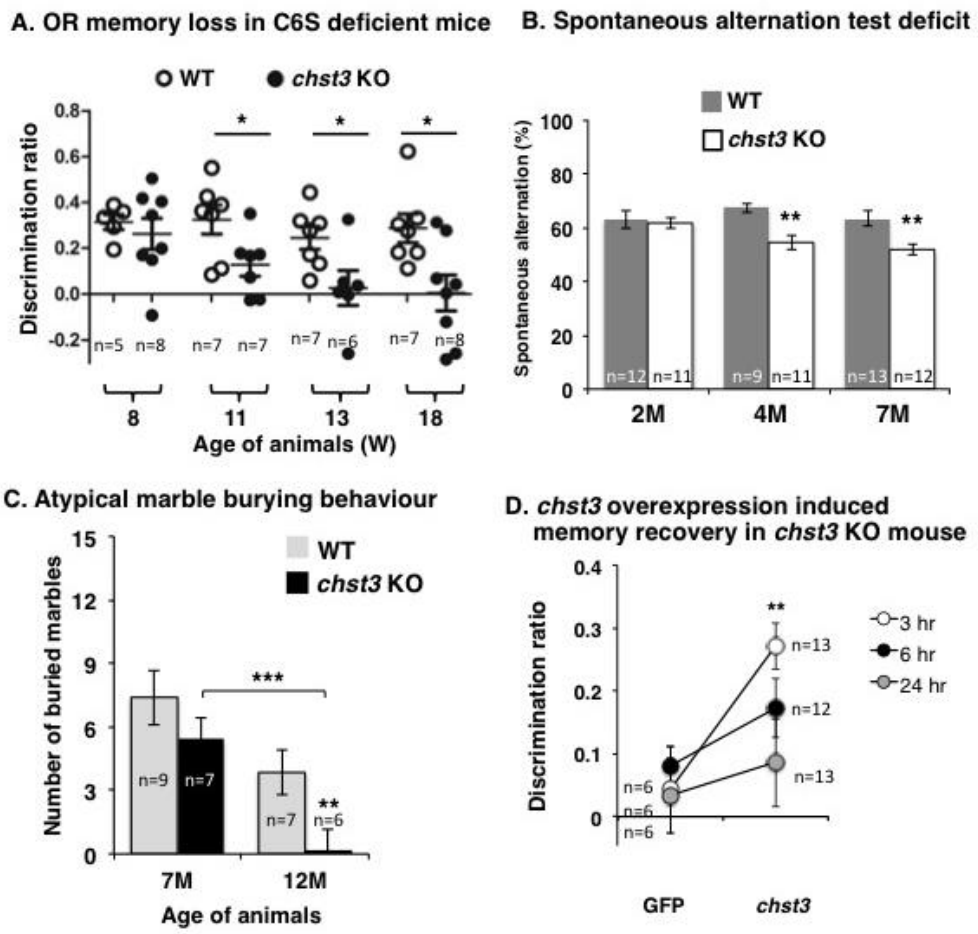

Fig. 2 Depletion of C6S leads to early memory loss and restoration of C6S reinstates aged memory

(A) OR memory loss (3 hr) in *chst3* knockout mice. Unpaired two-tailed t-test. 11W: *p=0.0317. 13W: *p=0.0306. 18W: *p=0.0165. W:weeks (B) Impaired spontaneous alternation performance in *chst3* knockout mice. Unpaired two-tailed *t*-test, 4M: **p=0.0011. 7M: **p=0.0023. (C) Atypical marble burying behaviour in *chst3* KO mice on ageing. Unpaired two-tailed t-test. 12M: **p<0.01. In *chst3* KO mice, the aging impaired marble burying behaviour, 7M vs 12M ***p<0.001 (D) *chst3* gene delivery recovered memory in 4M *chst3* KO mice line. Unpaired two-tailed *t*-test, 3hr delay: **p<0.01.

We next tested whether restoration of C6S would rescue memory in aged animals. Aged animals were tested for SOR at 19 months, demonstrating a profound memory deficit: these and 6M animals were injected with AAV1-*chst3* into PRh. 5 weeks later animals were tested again

(timeline Fig. S3C), showing restoration of NOR memory at the 3 and 6 hr time points almost to levels normally seen in young animals (Fig. 3A). C6S levels were increased in the injected region (Fig. S3D). The effect of increased C6S was also tested in transgenic animals overexpressing *chst3*, which have previously been shown to have enhanced plasticity as adults (*23*). This experimental group at 20M showed normal NOR 6h memory while the littermate group showed a deficit (Fig. 3B). Because the *chst3* expression in these transgenic mice is general rather than focal, we also tested SA memory and MB behavior, and found that the age-related decline in these tests was also prevented (Fig. S3E, F). These results support the idea that the level of C6S sulphation has a profound influence on memory, and that the age-related decline in C6S is a factor in age-related cognitive loss.

We show above that ageing influenced PV, with an increase in the number of high-expressing and decrease in low-expressing PV^+ cells, and a reversal of this pattern following ChABC treatment (Fig. 1D). A similar treatment effect was observed with AAV-*chst3* injections to the cortex (Fig. 3Ca), which additionally lowered WFA lectin staining of PNNs (Fig. 3Cb). In previous work, memory acquisition led to lowered PV caused by an increase in inhibitory inputs to PV^+ cells (*2*). We found a similar close inverse correlation between the number of inhibitory gephyrin synapses on PV^+ cells and their level of PV expression (Fig. 3E). In aged animals the overall number of gephyrin synapses on PV^+ cells was decreased compared to 6M animals, while treatment with AAV-*chst3* to restore C6S levels and memory led to restoration of the number of gephyrin synapses towards the level of young animals (Fig. 3D). These results suggest that aged inhibitory PNNs lead to a decrease in inhibitory inputs to PV^+ neurons, causing increased PV expression and increased cortical inhibition. Removing PNNs or restoring C6S levels enables increased inhibitory synapses on PV^+ interneurons, facilitating restoration of normal memory.

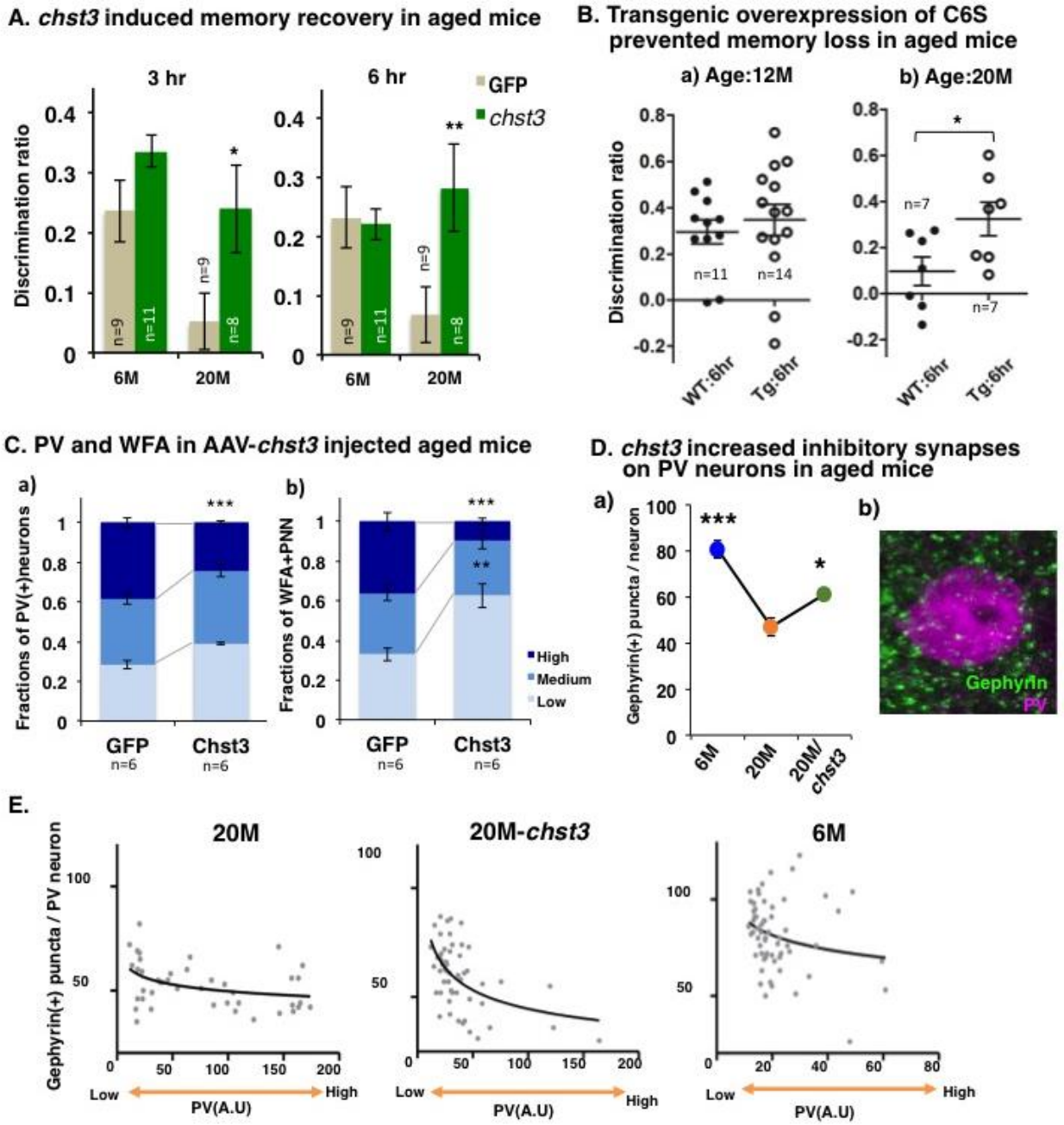

Fig. 3 (A) Age-mediated memory loss in C57bl/6 mice. 3hr memory retention: *p=0.023. 6 hr memory retention: **p=0.0071. (B) *chst3* transgenic mice prevented age-mediated memory loss. Age: 20M, 6hr memory retention: WT vs Tg *p=0.0361. Data present as mean ± SEM. (C) PV and WFA network in AAV-*chst3* injected aged mice a) PV network, High: ***p=0.0001 Low: n.s. p=0.079. b) WFA network, High: ***p<0.0001 Low: **p=0.0016. (D) *chst3* increased the inhibitory synapse on PV neurons in aged mice. a) n=6/group. 6M vs 20M ***p=0.0002. 20M vs 20M-*chst3*, * p=0.01. Unpaired two-tailed t-test. b) Staining profiles of gephyrin (+) synaptic puncta on PV cells. (E) Correlation profiles between numbers of gephyrin synaptic puncta and

PV intensity. 20M: Correlation *p=0.0186, Spearman r=-0.3576, 20M-Chst3: Correlation ***p=0.0003, Spearman r= -0.4717, 6M: Correlation *p=0.0364, Spearman r=-0.2686

The physiological effects of ageing and variations in C6S in the PRh and hippocampus were examined by recording long-term potentiation (LTP) and input/output curves in acute slices. *Chst3* knockout animals which have low C6S and memory loss, demonstrated a complete loss of LTP in layer II/III of PRh following temporal cortex stimulation and a similar loss in the hippocampus (Fig. 4A and B, left). The input/output relation was not changed (Fig. 4A and B, right). In aged animals, LTP in the cortex was diminished (Fig. 4C). However in AAV-*chst3* animals LTP was restored almost to the level of younger animals, but with no change in the input/output curve (Fig. 4C). These results are consistent with an overall higher level of inhibition in animals with low C6S levels, with previous evidence of PNN control of cortical excitability (*24*), and with previous evidence of increased inhibition in aged cortex (*25, 26*).

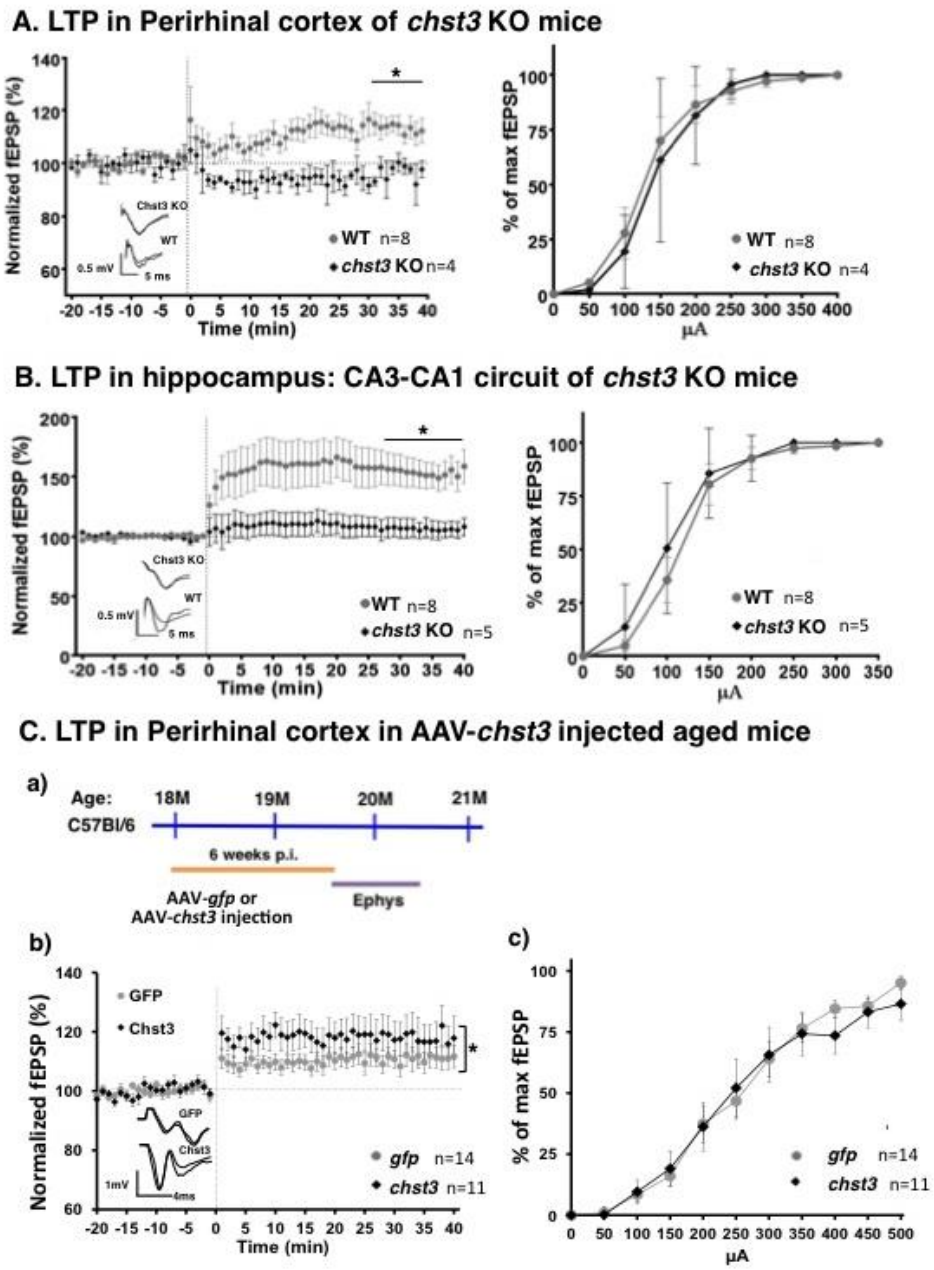

Fig. 4 Relation between C6S and long-term potentiation (LTP)

(A) LTP in perirhinal cortex slices in *chst3* KO mice. Left: LTP is significantly decreased (two-way RM ANOVA: *p=0.018). Left inset: Examples of fEPSP. Right: I/O curve of evoked fEPSP amplitude (two-way RM ANOVA, n.s. p=0.758;) (B) LTP is increased in CA3-CA1 in *chst3* KO mice (two-way RM ANOVA, *p=0.010). Left inset: Examples of fEPSP. Right: I/O curve (two-way RM ANOVA, n.s. p=0.457). Graphs are mean ± SEM. (C) LTP in perirhinal cortex in AAV-*chst3* injected aged mice. a) Time line. b) LTP in perirhinal cortex (two-way RM ANOVA: *p=0.036). Left inset: Examples of fEPSP. c) I/O curve (two-way RM ANOVA, $p > 0.05$).

The results of this study support the idea that CSPGs, particularly those in PNNs surrounding PV^+ interneurons, are involved in memory and cognition. The sulphation of these PNN CSs changes with ageing with the loss of C6S, rendering the PNN glycans more inhibitory (*16*, *27*), which decreases inhibitory connections on the dendrites and soma of inhibitory PV^+ interneurons (*3*). Digestion of PNN CS-GAGs, transgenic attenuation of PNNs and increased C6S therefore facilitate memory tasks, while loss of C6S due to ageing or deletion of *chst3* leads to diminished memory and cognition. These results demonstrate a mechanism for the loss of memory in the aged brain, and indicate that treatments targeting PNNs have the potential to ameliorate memory deficits associated with ageing.

References

1. D. C. Park, S. B. Festini, Theories of Memory and Aging: A Look at the Past and a Glimpse of the Future. *J Gerontol B Psychol Sci Soc Sci* **72**, 82-90 (2017); published online EpubJan (10.1093/geronb/gbw066).
2. F. Donato, S. B. Rompani, P. Caroni, Parvalbumin-expressing basket-cell network plasticity induced by experience regulates adult learning. *Nature* **504**, 272-276 (2013); published online Epub12/12/2013 (nature12866 [pii];10.1038/nature12866 [doi]).
3. P. Caroni, Inhibitory microcircuit modules in hippocampal learning. *Curr Opin Neurobiol* **35**, 66-73 (2015); published online EpubDec (10.1016/j.conb.2015.06.010).
4. J. J. Letzkus, S. B. Wolff, A. Luthi, Disinhibition, a Circuit Mechanism for Associative Learning and Memory. *Neuron* **88**, 264-276 (2015); published online EpubOct 21 (10.1016/j.neuron.2015.09.024).
5. B. A. Sorg, S. Berretta, J. M. Blacktop, J. W. Fawcett, H. Kitagawa, J. C. Kwok, M. Miquel, Casting a Wide Net: Role of Perineuronal Nets in Neural Plasticity. *J Neurosci* **36**, 11459-11468 (2016); published online EpubNov 09 (10.1523/JNEUROSCI.2351-16.2016).
6. T. Oohashi, M. Edamatsu, Y. Bekku, D. Carulli, The hyaluronan and proteoglycan link proteins: Organizers of the brain extracellular matrix and key molecules for neuronal function and plasticity. *Exp Neurol* **274**, 134-144 (2015); published online EpubDec (10.1016/j.expneurol.2015.09.010).
7. J. C. Kwok, J. P. Heller, R. R. Zhao, J. W. Fawcett, Targeting inhibitory chondroitin sulphate proteoglycans to promote plasticity after injury. *Methods Mol. Biol* **1162**, 127-138 (2014); published online Epub2014 (10.1007/978-1-4939-0777-9_10 [doi]).

8. J. Spatazza, H. H. Lee, A. A. Di Nardo, L. Tibaldi, A. Joliot, T. K. Hensch, A. Prochiantz, Choroid-plexus-derived Otx2 homeoprotein constrains adult cortical plasticity. *Cell Rep* **3**, 1815-1823 (2013); published online EpubJun 27 (10.1016/j.celrep.2013.05.014).
9. M. Ferrer-Ferrer, A. Dityatev, Shaping Synapses by the Neural Extracellular Matrix. *Front Neuroanat* **12**, 40 (2018)10.3389/fnana.2018.00040).
10. D. Rowlands, K. K. Lensjo, T. Dinh, S. Yang, M. R. Andrews, T. Hafting, M. Fyhn, J. W. Fawcett, G. Dick, Aggrecan directs extracellular matrix mediated neuronal plasticity. *J Neurosci* **38**, 10102-10113 (2018); published online EpubOct 3 (10.1523/JNEUROSCI.1122-18.2018).
11. C. Romberg, S. Yang, R. Melani, M. R. Andrews, A. E. Horner, M. G. Spillantini, T. J. Bussey, J. W. Fawcett, T. Pizzorusso, L. M. Saksida, Depletion of Perineuronal Nets Enhances Recognition Memory and Long-Term Depression in the Perirhinal Cortex. *J. Neurosci* **33**, 7057-7065 (2013); published online Epub4/17/2013 (33/16/7057 [pii];10.1523/JNEUROSCI.6267-11.2013 [doi]).
12. S. Yang, M. Cacquevel, L. M. Saksida, T. J. Bussey, B. L. Schneider, P. Aebischer, R. Melani, T. Pizzorusso, J. W. Fawcett, M. G. Spillantini, Perineuronal net digestion with chondroitinase restores memory in mice with tau pathology. *Exp. Neurol* **265**, 48-58 (2015); published online Epub3/2015 (S0014-4886(14)00383-5 [pii];10.1016/j.expneurol.2014.11.013 [doi]).
13. M. J. Vegh, C. M. Heldring, W. Kamphuis, S. Hijazi, A. J. Timmerman, K. W. Li, P. van Nierop, H. D. Mansvelder, E. M. Hol, A. B. Smit, R. E. van Kesteren, Reducing hippocampal extracellular matrix reverses early memory deficits in a mouse model of Alzheimer's disease. *Acta Neuropathol Commun* **2**, 76 (2014)10.1186/s40478-014-0076-z).
14. S. Yang, S. Hilton, J. N. Alves, L. M. Saksida, T. Bussey, R. T. Matthews, H. Kitagawa, M. G. Spillantini, J. C. F. Kwok, J. W. Fawcett, Antibody recognizing 4-sulfated chondroitin sulfate proteoglycans restores memory in tauopathy-induced neurodegeneration. *Neurobiol Aging* **59**, 197-209 (2017); published online EpubNov (10.1016/j.neurobiolaging.2017.08.002).
15. D. Carulli, J. C. Kwok, T. Pizzorusso, Perineuronal Nets and CNS Plasticity and Repair. *Neural Plast* **2016**, 4327082 (2016)10.1155/2016/4327082).
16. S. Foscarin, R. Raha-Chowdhury, J. W. Fawcett, J. C. F. Kwok, Brain ageing changes proteoglycan sulfation, rendering perineuronal nets more inhibitory. *Aging (Albany NY)* **9**, 1607-1622 (2017); published online EpubJun 28 (10.18632/aging.101256).
17. D. Carulli, T. Pizzorusso, J. C. Kwok, E. Putignano, A. Poli, S. Forostyak, M. R. Andrews, S. S. Deepa, T. Glant, J. W. Fawcett, Animals lacking link protein have attenuated perineuronal nets and persistent plasticity. *Brain* **133**, 2331-2347 (2010); published online Epub6/20/2010 (awq145 [pii];10.1093/brain/awq145 [doi]).
18. H. Wang, Y. Katagiri, T. E. McCann, E. Unsworth, P. Goldsmith, Z. X. Yu, F. Tan, L. Santiago, E. M. Mills, Y. Wang, A. J. Symes, H. M. Geller, Chondroitin-4-sulfation negatively regulates axonal guidance and growth. *J. Cell Sci* **121**, 3083-3091 (2008); published online Epub9/15/2008 (
19. S. Miyata, H. Kitagawa, Mechanisms for modulation of neural plasticity and axon regeneration by chondroitin sulphate. *J Biochem* **157**, 13-22 (2015); published online EpubJan (10.1093/jb/mvu067).
20. F. Donato, A. Chowdhury, M. Lahr, P. Caroni, Early- and late-born parvalbumin basket cell subpopulations exhibiting distinct regulation and roles in learning. *Neuron* **85**, 770-786 (2015); published online EpubFeb 18 (10.1016/j.neuron.2015.01.011).
21. S. S. Deepa, D. Carulli, C. Galtrey, K. Rhodes, J. Fukuda, T. Mikami, K. Sugahara, J. W. Fawcett, Composition of perineuronal net extracellular matrix in rat brain: a different disaccharide composition for the net-associated proteoglycans. *The Journal of biological chemistry* **281**, 17789-17800 (2006); published online EpubJun 30 (10.1074/jbc.M600544200).

22. R. Lin, T. W. Rosahl, P. J. Whiting, J. W. Fawcett, J. C. Kwok, 6-sulphated chondroitins have a positive influence on axonal regeneration. *PLoS. ONE* **6**, e21499 (2011); published online Epub2011 (10.1371/journal.pone.0021499 [doi];PONE-D-11-05800 [pii]).
23. S. Miyata, Y. Komatsu, Y. Yoshimura, C. Taya, H. Kitagawa, Persistent cortical plasticity by upregulation of chondroitin 6-sulfation. *Nat Neurosci* **15**, 414-422, S411-412 (2012); published online EpubMar (10.1038/nn.3023).
24. K. K. Lensjo, M. E. Lepperod, G. Dick, T. Hafting, M. Fyhn, Removal of Perineuronal Nets Unlocks Juvenile Plasticity Through Network Mechanisms of Decreased Inhibition and Increased Gamma Activity. *J Neurosci* **37**, 1269-1283 (2017); published online EpubFeb 1 (10.1523/JNEUROSCI.2504-16.2016).
25. M. Liguz-Lecznar, M. Lehner, A. Kaliszewska, R. Zakrzewska, A. Sobolewska, M. Kossut, Altered glutamate/GABA equilibrium in aged mice cortex influences cortical plasticity. *Brain Struct Funct* **220**, 1681-1693 (2015)10.1007/s00429-014-0752-6).
26. H. E. Rossiter, E. M. Davis, E. V. Clark, M. H. Boudrias, N. S. Ward, Beta oscillations reflect changes in motor cortex inhibition in healthy ageing. *Neuroimage* **91**, 360-365 (2014); published online EpubMay 1 (10.1016/j.neuroimage.2014.01.012).
27. S. Miyata, H. Kitagawa, Formation and remodeling of the brain extracellular matrix in neural plasticity: Roles of chondroitin sulfate and hyaluronan. *Biochim Biophys Acta*, (2017); published online EpubJun 15 (10.1016/j.bbagen.2017.06.010).

Methods and materials

Mice

The normal wild type (WT) C57BL/6J (Charles river, UK) mice were used for ChABC treatment study and 6M of age represents for young adults and 20M for aged group. In order to test between C6S and memory, two transgenic mouse models were used; c6st-1 (encoded by chst3 gene) knockout mice (21) and chst3-1 overexpressing Tg mice (22). Age-matched littermates were used as control mice. Animals had unrestricted access to food and water, and were maintained on a 12 hr light/dark cycle (lights off at 7:00 P.M.). All experiments were carried out in accordance with the UK Home Office Regulations for the Care and Use of Laboratory Animals and the UK Animals (Scientific Procedures) Act 1986.

Generation of adeno-associated viral vectors

The plasmid encoding AAV-PGK-chst3 was made by amplifying the mouse chst3 sequence from plasmid MR207541 (OriGene) via the primers 5’ GGAATTCATAGGGCGGCCGGGAA 3’ and 5’ AGCGCTGGCCGGCCGTTTAAAC 3’ and was cloned into plasmid AAV-PGK-Cre (Addgene plasmid # 24593) between the AfeI (NEB, R0652) and EcoRI (NEB, R0101) sites to substitute the Cre recombinase gene. The eGFP sequence of AAV-CMV-eGFP (Addgene plasmid # 67634) was amplified by using the primers 5’ GGAATTCATGGTGAGCAAGGGCGAG 3’ and 5’ AGCGCTTTACTTGTACAGCTCGTCCATG 3’, which was next cloned into the digested

AAV-PGK-backbone. These virus vectors were turned into a recombinant adeno-associated viral vector with serotype 1 as described in previously published protocol (J. Verhaagen et al., 2018). For the present study, the following vectors were produced: AAV1-PGK-*chst3* $1.44x10^{12}$ gc/ml; AAV1-PGK-GFP $1.42x10^{12}$ gc/ml; AAV1-SYN-GFP $8.99x10^{12}$ gc/ml

J. Verhaagen et al., Small Scale Production of Recombinant Adeno-Associated Viral Vectors for Gene Delivery to the Nervous System. Methods Mol. Biol. 1715, 3–17 (2018).

Animal surgeries

Animal surgeries were performed under isoflurane anesthesia. ChABC (50 U/ml in PBS, Seikagaku), or AAV vectors (AAV1-PGK-Chst3 or AAV1-PGK-GFPor AAV1-SYN-GFP) was stereotaxically injected to six different sites in the PRh ($1x10^8$ particles in total, 3 per hemisphere, 0.5 µl with a speed of 0.2 µl/min). Injections were made with a 10 µl Hamilton syringe and a 33 gauge needle at the following sites (in mm from bregma and the surface of skull): 1. anteriorposterior (AP): -1.8; lateral (L): ± 4.6; ventral (V): -4.4. 2. AP: -2.8; L: ± 4.8; V: -4.3. 3. AP: -3.8; L: ± 4.8; V: -3.8. The needle remained in place at the injection site for 3 min before being slowly withdrawn over 2 min. AAV1-SYN-GFP was injected as a control viral vector for chst3 gene delivery to chst3 KO mice.

Spontaneous Object Recognition task

The spontaneous object recognition (SOR) task was performed as previously described for mice (Yang et al, 2015). Briefly, all mice were habituated in three consecutive daily sessions in the empty Y-maze apparatus for 5 min after recovery from surgery. Each test session consisted of a sample phase and a choice phase. In the sample phase, the animal was placed in the start arm and left to explore two identical objects, which were placed on the end of two arms for 5 min. The choice phase followed after a delay of either 1 min, 3 hr, 6 hr as a short-term memory paradigm or 24 hr and 48 hr as a long-term memory paradigm, which the animal spent in the home cage. The choice phase was procedurally identical to the sample phase, except that one arm contained a novel object, whereas the other arm contained a copy of the repeated object. When the animals were assessed, a different object pair was used for each session for a given animal, and the order of exposure to object pairs were counterbalanced within and across groups. All the sessions were recorded by a technician (SH) who is blind to the genotype. The object exploration time was assessed from video recordings of the sample and choice phase by scorer (SY) blind to the genotype of the mouse. The direct nasal or head contacts only were regarded as an exploratory behaviour. A discrimination ratio was calculated by dividing the difference in exploration of the novel and familiar objects by the total object exploration time. Therefore, the discrimination ratio varies from 0 (equal exploration for novel and familiar objects) to 1 (exploration of the novel object only). The test sessions were separated by a minimum of 48 hr. One-way analysis of variance (ANOVA) followed by Tukey post hoc test was used for comparisons of multiple

groups with a significance level of $p < 0.05$, using GraphPad Prism version 5.0. An unpaired two-tailed t-test was used for two-group comparisons.

The minimum sample size per animal experiment required to have meaningful results was 14 animals, which was calculated based on raw data of chABC or control treated 20M old mice using following parameters; type 1 error rate (a):0.05 and power: 0.8 , mu1 -0.002, mu 2 0.3301, sigma 0.214 (http://www.stat.ubc.ca/~rollin/stats/ssize/n2.html).

For some experiments two cohorts of mice were recruited and the results were analysed at the end of experiments.

Spontaneous alternation test

The Y maze was made by three white, opaque Perspex plastic arms (8 cm width, 20 cm length, 35 cm height) at a 120° angle from each other. There were no visual cues inside the maze. Each animal was allowed to freely navigate all three arms for 5 min after placing it at the centre of multiple arms via a tube. The number of arm entries and the number of triads were recorded in order to calculate the percentage of alternation. An entry occurs when all four limbs are within the arm. The inside of Y maze was cleaned with 50% ethanol between trials and allowed to dry.

Marble burying test

Standard polycarbonate rat cages (26 cm x 48 cm x 20 cm) with fitted filter-top covers was used as a testing chamber and fresh, unscented mouse bedding material to each cage to a depth of 5 cm. Glass toy marbles (assorted styles and colors, 15 mm diameter, 5.2 g in weight) were placed gently on the surface of the bedding in 3 rows of 5 marbles. Each animal was carefully placed into a corner of the cage containing marbles, as far from marbles as possible, and the lid was placed on the cage and remained for 30 min. Marble as buried if two-thirds of its surface area is covered by bedding was counted by a scorer blind to the genotype of the mouse.

Immunohistochemistry

Diaminobenzidine (DAB) staining

Sample preparations and the general procedures of immunostaining have been described previously (Yang et al., 2015). In general, 30 µm free floating sections were incubated with 10 % methanol, 3 % H_2O_2 in PBS for 20 min at room temperature for quenching endogenous peroxidase activity. Sections were rinsed three times in 0.2 % Triton-X in PBS (PBS-T) and were subsequently blocked with 5 % normal goat serum (NGS) or normal horse serum (NHS) in PBS-T for 1 hr at room temperature. The primary antibodies (PV; 1:1000, Swant; Biotin-WFA; 1:100, Sigma-Aldrich) were incubated over night at 4 °C following rinsing tissues for 5 min

three times in PBS-T (0.2 % Triton-X in PBS). For Sema3A staining, as adapted from Vo et al, 2013, tissue sections were pre-incubated with 0.1 U/ml of ChABC (Seikagaku) in ChABC buffer (0.1 M Tris-HCl, 0.03 M sodium acetate, pH 8.0) for 2 hr at 37 °C prior to quenching. Then Sema3A antibody (1:50; Santa Cruz Biotechnology) was incubated overnight at room temperature. Following 3 washes in PBS-T they were incubated for 2 hr at RT with the appropriate biotinylated secondary antibody (Vector Laboratories) diluted 1:500 in PBS-T. Subsequently, sections were incubated with an avidin-biotin system (Vectastain; Vector Laboratories) for 1 hr at room temperature and washed with PBS-T. The immunostaining was visualized with DAB with 3 % H_2O_2 (DAB kit; Vector Laboratories) for 1-5 min at room temperature. For Sema3A staining the immunolabelling was performed with DAB with 0.3 % H_2O_2 for 10-20 min at room temperature. The sections were mounted on gelatin-coated slides and air-dried. Following dehydrating tissue sections in ascending concentration of alcohols, they are cleared in xylene and coverslipped with DPX. The tissue sections were examined using a light microscope and photographed using a digital camera (Leica DM6000 Microsystems).

Fluorescent staining/Analysis

Sections were blocked with 5 % normal goat serum (NGS) or normal horse serum (NHS) in PBS-T for 1 hr at RT. The primary antibodies (PV; 1:1000, Swant CS56; 1:100, Sigma-Aldrich; Biotin-WFA; 1:100, Sigma-Aldrich, Gephyrin; 1:200, Synaptic system) were incubated overnight at 4 °C. Following 3 washes in PBS they were incubated for 2 hr at RT with the appropriate secondary antibody conjugated with Alexa fluor 647, Alexa fluor 488 or Alexa fluor 568 or Streptavidin-Alexa fluor 647 (Molecular Probes, Invitrogen) diluted 1:500 in PBS-T. incubated with secondary antibodies for 2 hours. Sections were rinsed and mounted on 1% gelatin coated slides with FluorSave™ Reagent (Merck Millipore, Germany).

For synaptic puncta quantification images were captured using a Leica SPE confocal microscope using x63 objectives with a 1024 x 1024 image resolution (n=6 per group). At least 3 z-stack images (total 5 µm) were taken per section with at least 3 sections analyzed per animal (approx. 360µm apart). Images contained at least 5 PV positive neurons. At least 50 PV^+ neurons per animal were analysed for gephyrin (+) puncta quantification. Synaptic puncta analysis was performed with an automated custom script using an imageJ 1.29 plugin (available from c.eroglu@cellbio.duke.edu) (Ippolito and Eroglu, 2010).

Ippolito DM, Eroglu C. Quantifying Synapses: an Immunocytochemistry-based Assay to Quantify SynapseNumber. J. Vis. Exp JoVE. 45, 2270 (2010).

Electrophysiology

Animals were anesthetized with isoflurane and decapitated. The brain was rapidly removed and placed in ice-cold cutting solution bubbled with 99% O_2 containing the following (in mM): 126 NaCl, 2.5 KCl, 1 $CaCl_2 \cdot H_2O$, 2 $MgCl_2$, 1.25 $NaH_2Po_4 \cdot H_2O$, 10 $NaHCO_3$, 5 D-glucose, 0.4 ascorbic acid, 3 myoinositol, 3 pyruvate, and 15 HEPES, adjusted to pH 7.35. For perirhinal

cortex a midsagittal section was made and the rostral part of one hemisphere was cut at 45° to the dorsoventral axis (Cho et al., 2000). The cerebellum was removed from the brain with a further caudal coronal cut. The hemisphere was glued by its rostral end to a Vibratome stage (VT 1000S; Leica). Slices (380 □m) of perirhinal cortex were taken in the region -2.5mm to -4mm rostral from bregma. For hippocampus the whole brain was glued by its caudal end and coronal sections were taken in the region of dorsal hippocampus. Slices were stored submerged in bubbled, artificial CSF (20-25°C, same composition as cutting solution, except 2 mM $CaCl_2$, 1 mM $MgCl_2$ and without: ascorbic acid, myoinositol, pyruvate) for 2 hr before the onset of recordings. A single slice was placed in an interface recording chamber superfused by artificial CSF (30°C, flow rate 2 ml/min). Evoked field EPSPs (fEPSP) for perirhinal cortex were recorded from layers II/III from directly below the rhinal sulcus (area 35). A stimulation electrode was placed in layer II/III on the entorhinal side (0.5 mm, area 36) of the recording electrode (Cho et al., 2000). fEPSP for hippocampus were recorder placing the stimulation electrode in the stratum radiatum of the CA3 field and the recording electrode in the same layer of the CA1 field. Stimuli (0.1 ms duration) were delivered to the stimulation electrode at 0.1 Hz. Input/output curves were produced with stimulation intensities from 50 to 450 □A in steps of 50 □A. For monitoring baseline synaptic transmission before LTP induction, fEPSPs were reduced to 40-50 % of the maximum amplitude and recorded for at least 20 min or until responses were stable (< 20 % amplitude change over 30 min). For LTP induction, the following protocol was used: 4 bursts at interval of 15 s, each composed by 10 trains at interval of 0.2 s, each composed by 4 pulses at interval of 10 ms and of 0.2 ms of duration with 3 V of amplitude. Subsequently, fEPSPs elicited by stimulations at interval of 20 s were recorded for further 40 min. Field potentials were amplified with a CyberAmp 320 (Molecular Devices) and recorded and analyzed with custom-made software written in LabView (National Instruments). For offline LTP analysis, fEPSPs were averaged across 1 min and the peak amplitude of the mean fEPSP was expressed relative to the preconditioning baseline. The significance of group means was established using repeated-measures (RM) ANOVA.

Supplementary figures

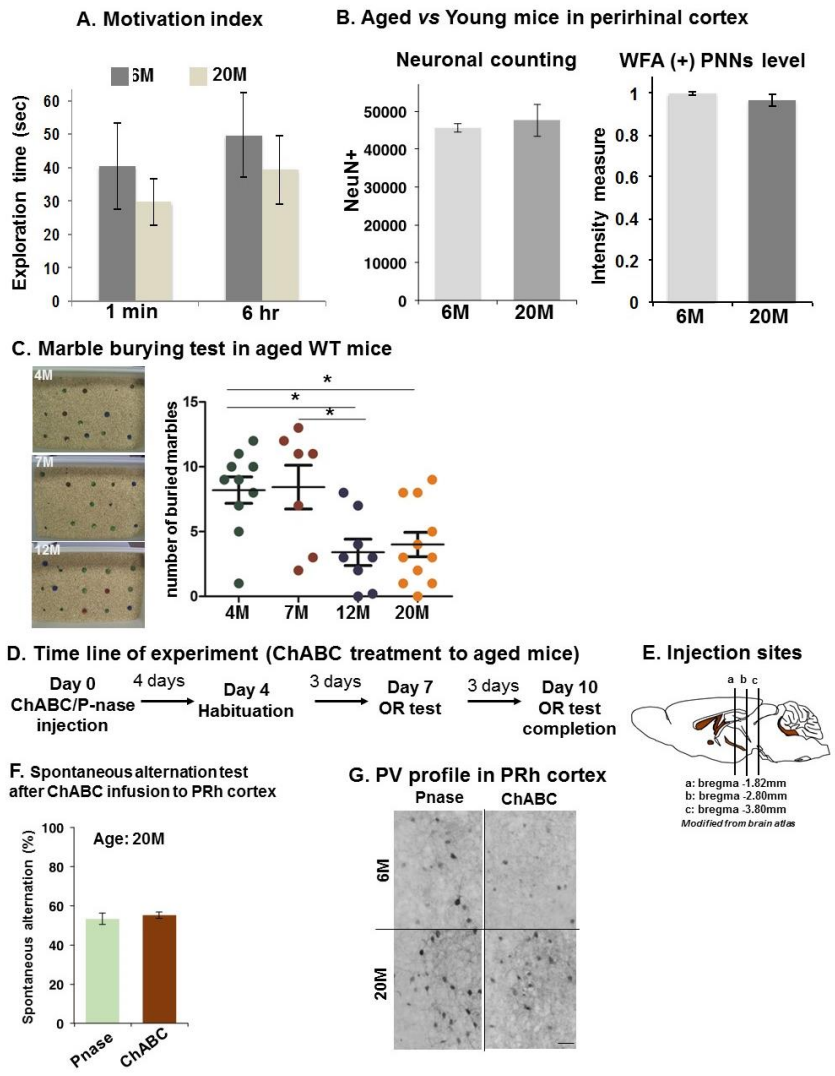

Supplementary Fig.1 (A) Motivation index indicated by exploration time during sample phase of NOR test. No significant alteration in motivation was displayed between young and aged mice groups. 6M n=4, 20M n=7 (B) Neuronal counting (Left) and WFA(+) PNNs level (Right) in the perirhinal cortex of 6M or 20M old C57bl/6 mice. NeuN(+): n=6/group, WFA(+): n=4/group. (C) Marble burying test in C57bl/6 at different ages, Left: representative images of marble burying test Right: 4M n=10, 4M n=6, 7M n=8, 20M n=11, One-way ANOVA **p=0.004, Tukey post hoc test, 4M vs 12M *p<0.05, 4M vs 20M *p<0.05, 7M vs 12M *p<0.05, Data represents as mean ± SEM. (D) ChABC treatment to aged mice, 19M-old C57bl/6 mice were used. After 4 days of treatment, habituation of NOR test was performed and OR memory was measured at 7 days post injection. (E) ChABC or Pnase injections to perirhinal cortex. It is a schematic illustration of sagittal section of murine brain. a: bregma -1.82mm b: bregma -2.8mm c: bregma -3.8mm (F) Spontaneous alternation performance after ChABC treatment to perirhinal cortex (PRh) in aged mice. (G) Immunohistochemistry of PV in PRh cortex after ChABC or Pnase injection. Scale bar: 50 µm

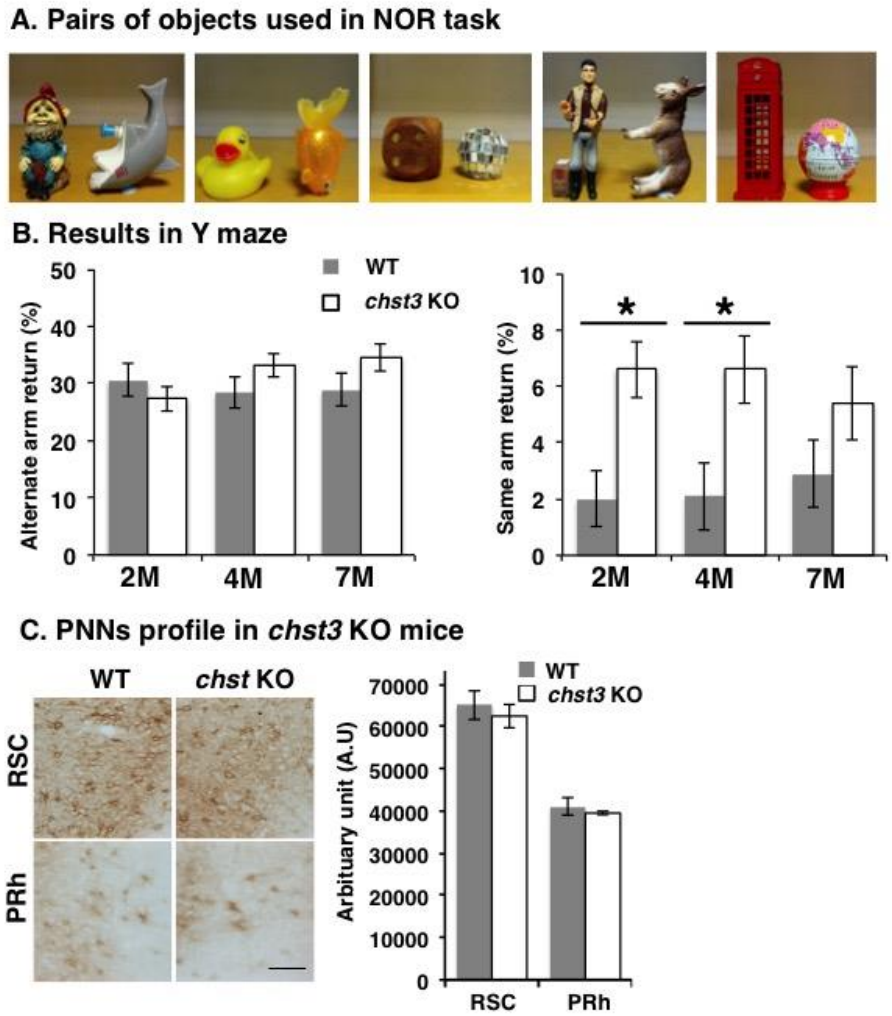

Supplementary Fig.2

(A) Pairs of objects used in SOR task. (B) Y-maze based spontaneous alternation test in *Chst3* KO mice at different ages, 2M: WT n=8, *chst3* KO n=16, 4M: WT n=9, *chst3* KO n=11, 7M: WT n=12, *chst3* KO n=12. Left: Alternate arm return, Right: unpaired two-tailed t-test 2M: *p=0.018 4M: *p=0.019, 7M: n.s. p=0.2 (C) Analysis of PNNs in chst3 KO mice, Left: Immunohistochemistry of WFA(+) profile in retrosplenial cortex (RSC) and perirhinal cortex (PRh). Scale bar: 50 µm Right: WFA intensity comparison between WT and *chst3* KO mice. There is no significant difference between WT and *chst3* KO. n=6/group, Data represents as mean ± SEM.

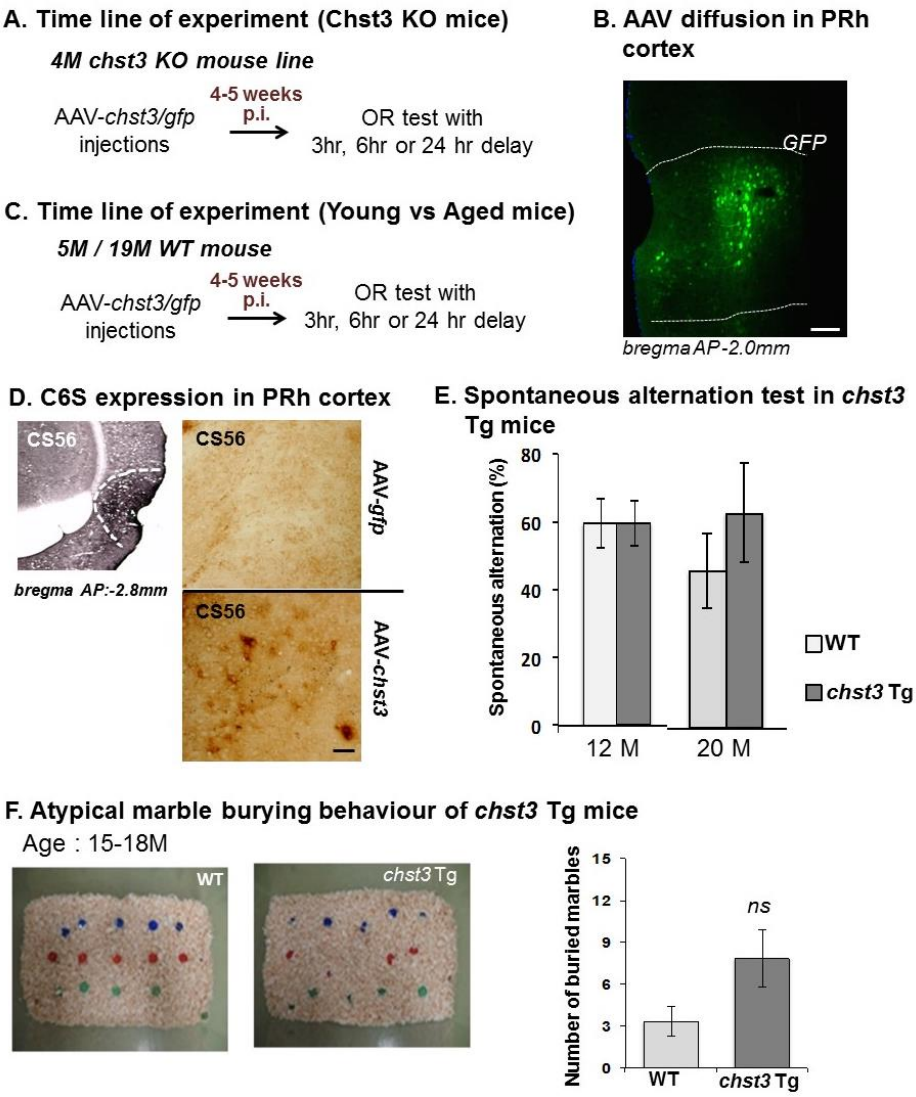

Supplementary Fig.3

(A) Experimental time line of AAV-*chst3* injection to *chst3* KO mice at 4M. The viral vectors were injected to the perirhinal cortex and OR memory was tested at 4-5 weeks post injection. (B) The profile of AAV-GFP diffusion in perirhinal cortex, Scale bar: 100 µm (C) Experimental time line of AAV-*chst3* injection to 5M or 19M C57bl/6 mice. The viral vectors were injected to the perirhinal cortex and OR memory was tested at 4-5 weeks post injection. (D) C6S expression induced by AAV-*chst3* was detected by CS56 antibody in WT mice at 20M. AAV-GFP injection has no CS56 positive staining. Scale bar: 50 µm (E) Spontaneous alternation test in *chst3* Tg mice Age: 12M, WT n=5, *chst3* Tg n=9. Age: 20M, WT n=4 and *chst3* Tg n=4. There is no difference between WT and *chst3* Tg mice at 12M and 20M. (F) Marble burying behaviour of *chst3* Tg mice at the age of 15-18M. Left: representative images of marble burying test Right: WT n=6, *chst3* Tg n=6